Extra-large pore zeolite (ITQ-40) with the lowest framework density containing double four- and double three-rings

A. Corma[a], M. J. Díaz-Cabañas[a], J. Jiang[a], M. Afeworki[b], D. L. Dorset[b], S. L. Soled[b], and K. G. Strohmaier[b]

[a]Instituto de Tecnología Química, CSIC-Universidad Politécnica de Valencia, Valencia, Spain; and [b]Corporate Strategic Research, ExxonMobil Research and Engineering Company, Annandale, NJ

Edited* by Mark E. Davis, California Institute of Technology, Pasadena, CA, and approved May 17, 2010 (received for review March 11, 2010)

The first zeolite structure (ITQ-40) that contains double four (D4) and double three (D3) member ring secondary building units has been synthesized by introducing Ge and NH_4F and working in concentrated synthesis gels. It is the first time that D3-Rs have been observed in a zeolite structure. As was previously analyzed [Brunner GO, Meier, WM (1989) *Nature* 337:146–147], such a structure has a very low framework density (10.1 T/1,000 Å^3). Indeed, ITQ-40 has the lowest framework density ever achieved in oxygen-containing zeolites. Furthermore, it contains large pore openings, i.e., 15-member rings parallel to the [001] hexagonal axis and 16-member ring channels perpendicular to this axis. The results presented here push ahead the possibilities of zeolites for uses in electronics, control delivery of drugs and chemicals, as well as for catalysis.

double three-rings in zeolites | low framework density zeolites | germanosilicate zeolites

There is an increasing interest in the synthesis of zeolites with low framework density and extra-large pores (>12 tetrahedral atoms). The preparation of such materials will increase the use of zeolites in catalysis (1, 2) while further expanding their possibilities in microelectronics by preparing materials with low values of the high-frequency dielectric constant, or for uses related with controlled delivery of chemicals and diagnostic treatment (3, 4).

In 1989, Brunner and Meier performed a topological analysis on synthesized zeolites and aluminophosphates with four-connected frameworks (5). They found that when the frameworks were grouped as a function of the smallest ring present in the structure, the minimum framework density calculated for each of the groups decreases with the smallest ring size. These results suggested that one way of preparing low framework density zeolites could be to build structures with four- and three-rings. Following this suggestion and the recognition that several beryllium-containing natural zeolites, such as lovdarite and nabesite, have three-rings in their structures, Cheetham et al. (6) prepared a large pore ($14 \times 8 \times 8$) zeolite with Be that contains three-rings. Previously, Davis et al. considered using zinc as a framework cation to promote the formation of three-rings, and while three zincosilicates containing three-rings were subsequently synthesized, none of them contain extra-large pores (7–9). Later, we have shown by theoretical and experimental work, that Ge has a directing effect toward the formation of double four-rings (D4Rs) (10, 11), and the presence of these secondary building units (SBUs) has allowed the synthesis of several large and extra-large pore zeolites (12–15). Among those, Instituto de Tecnologia Química number 33 (ITQ-33) contains D4Rs and three-ring units in the structure and has a low framework density (12.3 T/1,000 Å^3). Very recently, an interrupted zeolite with a three-dimensional mesoporous channel system (ITQ-37) has been presented (16), which contains D4Rs and has the lowest framework density reported (10.3 T/1000 Å^3). Taking this into account, one could expect that the framework density will decrease even more if zeolites with structures with D4R and double three-ring (D3R) could be obtained. While D3R SBUs have been observed in organic-containing silicate clathrates (17) and as molecular species in silicate mixtures [especially those with tetraethylammonium cations (18)], they have never been observed in synthesized zeolites, probably due to the strain involved within this SBU.

Here we will show the synthesis and structure of an extra-large pore ($16 \times 15 \times 15$) zeolite (ITQ-40) whose framework is built from three secondary building units, consisting of (*i*) $[6^4 5^3 4^3 3]$ cages connected along *a* and *b* axes by (*ii*) D4Rs and along the *c* axis by (*iii*) D3Rs. This work shows the possibility of building D3Rs within a zeolite structure, which has resulted in the silicate zeolite with the lowest framework density (10.1 T/1,000 Å^3).

Results and Discussion

Zeolite Synthesis. Zeolite ITQ-40 has been obtained from germanium containing gels in fluoride media with the objective of stabilizing D4Rs. Preliminary theoretical calculations indicate that germanium can also stabilize D3Rs, which otherwise would be quite unstable when formed only by silicon.

As structure directing agents we have used two diphenyldialkylphosphonium derivatives, in which the two alkyl groups were dimethyl or diethyl. The synthesis of the organic structure directing agents (SDAs) as well as the yield obtained in each case is given in *SI Text*.

Although it is possible to synthesize ITQ-40 with dimethyldiphenylphosphonium (Me_2Ph_2POH) as SDA, diethyldiphenylphosphonium (Et_2Ph_2POH) is a more convenient SDA because it is then possible to obtain pure ITQ-40 in a wider range of compositions in a very reproducible way. Then, a study on the influence of the synthesis variables using Et_2Ph_2POH as SDA (see Table 1) was carried out with a general gel composition:

$$(1\text{-}a)\,SiO_2 : a\,GeO_2 : b\,T^{III}{}_2O_3 : 0.4\,SDA(OH) : 0.4\,NH_4F : c\,H_2O.$$

The Si/Ge ratio was varied between 1 and 15, the T^{III}/T^{IV} ratio was 30, T^{III} being aluminum or boron, and the H_2O/T^{IV} ratio varied between 1 and 15. The syntheses were carried out at 175 °C under static conditions. The synthesis time was 1 day for samples with Si/Ge = 1 and 14 days for the rest of the experiments. As can be seen in Table 1, ITQ-40 was obtained only with highly concentrated gels ($H_2O/T^{IV}O_2 = 1$) and with a Si/Ge ratio of 1 (Fig. 1). The chemical analysis of the pure ITQ-40 yields a Si/Ge ratio of up to 1.40. Both Al and B could be incorporated in the zeolite as per chemical analysis, and the presence of Al^{IV} will be shown by means

Author contributions: A.C. and M.J.D.-C. designed research; J.J., M.A., D.L.D., S.L.S., and K.G.S. performed research; A.C., M.J.D.-C., M.A, D.L.D., S.L.S., and K.G.S. analyzed data; and A.C. and K.G.S. wrote the paper.

The authors declare no conflict of interest.

*This Direct Submission article had a prearranged editor.

[1]To whom correspondence should be addressed. E-mail: acorma@itq.upv.es.

This article contains supporting information online at www.pnas.org/lookup/suppl/doi:10.1073/pnas.1003009107/-/DCSupplemental.

Table 1. Influence of synthesis variables with Et_2Ph_2POH as SDA

			F = 0.4			OH = 0.4	
			$T^{III} = 0$	Al = 0.033	B = 0.033	$T^{III} = 0$	Al = 0.033	B = 0.033
Si/Ge = 1	H_2O	1						
		5						
		15						
Si/Ge = 5	H_2O	1						
		5						
		15						
Si/Ge = 15	H_2O	1						
		5						
		15						

In the table, red represents ITQ-40, yellow represents ITQ-40 + ITQ-31, purple represents ITQ-40 + Quartz (GeO_2), green represents Amorphous + ITQ-40, blue represents Amorphous, and gray represents ITQ-31 + Quartz (GeO_2).

of ^{27}Al magic angle spinning (MAS) NMR. For Si/Ge = 5 in the gel, a small amount of ITQ-40 starts to grow, but crystallization does not continue even after 14 days, while another phase starts to grow (see Fig. S1).

We have made some attempts to perform the synthesis in OH media and in absence of fluoride with the following gel composition

$$(1\text{-}a)\,SiO_2 : a\,GeO_2 : b\,T^{III}{}_2O_3 : 0.25\,SDA(OH) : 7\,H_2O.$$

Under these conditions, only ITQ-31 plus GeO_2 and amorphous germanosilicates were observed.

After removing the SDA by calcination in air at 540 °C, the Horvath–Kawazoe formalism (19) over Ar adsorption measurements was applied to ITQ-40, showing the presence of one of the pores centered at 10.0 Å of diameter and a second at 7.7 Å (Fig. S2). Nitrogen adsorption measurements gave a Brunauer–Emmitt–Teller (BET) surface area of 535 m^2/g and 0.16 cm^3/g of micropore volume. The results indicate that the pure silica polymorph will have 708 m^2/g of BET area and 0.21 cm^3/g of micropore volume based on the lower atomic weight of silicon compared to germanium. From Ar and N_2 adsorption results, we can conclude that ITQ-40 must be an extra-large pore zeolite with two pores of different dimensions and with a low framework density.

The ^{29}Si MAS-NMR spectrum (Fig. 2) of the as-synthesized sample shows a large amount of defects (silanols), suggesting the presence of incompletely connected T sites (tetrahedral sites). The signal corresponding to silanols is shown as enhanced by ^{1}H cross-polarized magic angle spinning (CPMAS) NMR (Fig. 2 *Inset*). The results indicate that the fraction of the incompletely connected T atoms from the quantitative MAS spectrum corresponds to 9.6% of the total Si.

^{19}F MAS NMR gives a characteristic band at −38 ppm when F is located within pure silica D4Rs (20), this band being a direct proof of the presence of D4R units in the structure. However, when Ge is also present in D4Rs, the band shifts to higher field depending on the Si/Ge ratio (11). The presence of a signal at −6.5 ppm in the ^{19}F MAS-NMR spectra of the ITQ-40 sample (Fig. 3) proves the presence of germanium -rich D4R in the structure.

When Al was introduced in the synthesis gel, as presented in Table 1, the resultant ITQ-40 contains aluminum, as determined by chemical analysis. ^{27}Al MAS-NMR spectrum presents a strong band at 48 ppm (Fig. S3*A*) that can be assigned to tetrahedrally coordinated Al and can be associated to the presence of framework Al. A band corresponding to octahedrally coordinated Al (~0 ppm) is also present.

The ^{31}P MAS-NMR spectrum (Fig. S3*B*) of the as-synthesized sample indicates the presence of two types of ^{31}P species. The SDA appears to remain intact in the as-synthesized ITQ-40 sample as evidenced by ^{13}C NMR spectra (Fig. S4).

Structural Solution. Like other germanium-containing crystalline oxide materials, ITQ-40 is not stable once the organic template is removed by calcination in air. This is due to the reactivity of the tetrahedral germanium oxide bonds that are quickly hydrolyzed by ambient water in the air. The presence of the SDA stabilizes the framework and prevents structural collapse as long as it remains inside the pores of the framework. The SDA may also restrict the access of water molecules to the germanium sites. Most pure silica analogs of zeolites, on the other hand, do not react with water and retain their crystalline structure after the SDA has been removed. For these reasons the initial structural solution was attempted from powder diffraction on the as-synthesized form.

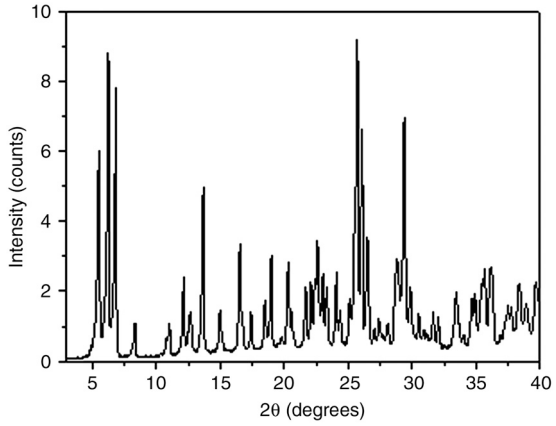

Fig. 1. X-ray diffraction pattern of as-made ITQ-40 zeolite.

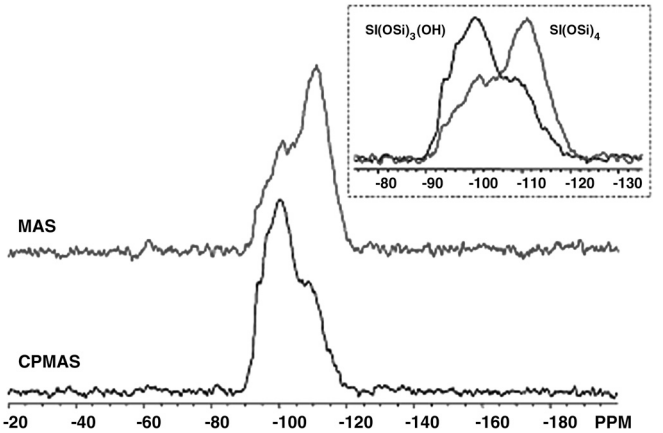

Fig. 2. NMR spectra of as-synthesized ITQ-40: 99 MHz ^{1}H-to-^{29}Si CPMAS (*Bottom*) and ^{29}Si MAS (Bloch decay, *Top*). (*Inset*) An overlay of the CPMAS and MAS-NMR spectra. About 9.6% of the total signal in the MAS spectrum is in a region where silanol species are observed. These regions are preferentially enhanced in the CPMAS spectrum.

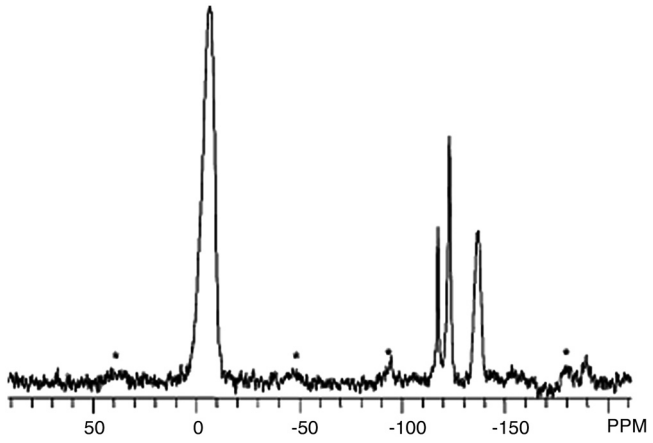

Fig. 3. ^{19}F MAS NMR of as-synthesized ITQ-40. The dominant signal at −6.5 ppm indicates the presence of germanium-rich D4R in the structure. Spinning sidebands are shown with asterisks.

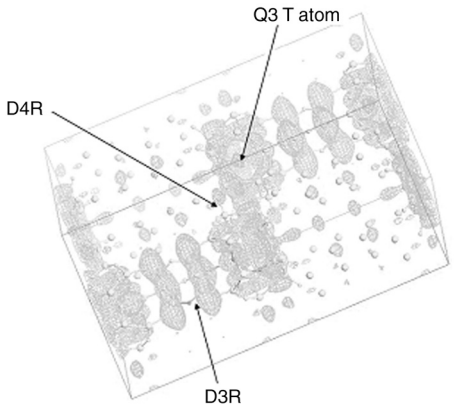

Fig. 4. Direct methods solution of ITQ-40 from electron diffraction with superimposed final model. The map shows the fit of the framework atoms to the electrostatic potential map of the as-synthesized material (Fourier transform of combined direct methods phases with electron diffraction amplitudes).

Initial attempts to index the powder X-ray pattern from as-synthesized ITQ-40 were successful, indicating a hexagonal unit cell where $a = 16.41$, $c = 32.33$ Å. Two orthogonal zones of electron diffraction data (hk0 + 0kℓ) supported these dimensions [$a = 16.42(10), c = 31.90(8)$ Å] and symmetry. Detected systematic absences of reflections supported space group $P6_3/mmc$ (#194) (21), along with reflection class equivalencies, assuming the underlying structure to be centrosymmetric.

The observed structure factors, |Fobs|, were then computed from a full profile LeBail extraction (22) of the peak intensities from the X-ray powder pattern. These data were then used in repeated attempts to solve the structure by the *FOCUS* (23) algorithm, an automated method of structure determination using crystal chemical information, but no suitable trial models were found.

The next attempt at structure determination was from electron diffraction data by using direct methods to assign crystallographic phases from 98 combined hk0 and 0kℓ electron diffraction amplitudes by maximum entropy and likelihood via the MICE program. A possible structure solution was found in the most likely ranked crystallographic phase sets. The overall electrostatic potential map (Fig. 4), as well as similar unit cell dimensions and space group symmetry, suggested a relationship with existing UCSB-6GaCo (**SBS**) (24) and EMC-2 (**EMT**) (25) zeolite frameworks, at least in the arrangement of nonframework porous space. As will be shown, the density sites in the electron crystallographic solution correspond well to T-site (tetrahedral site) position identified in subsequent X-ray analyses.

A partial structure was subsequently determined from the powder X-ray data of the as-synthesized material using the program Powder-Solve (26), derived partially from the simulated annealing method developed by Deem and Newsam (27). This method involves placing atoms at random positions in the unit cell and then adjusting their atomic coordinates in an iterative manner using simulated annealing such that the calculated X-ray powder diffraction pattern most closely resembles the experimental powder pattern intensity profile. The first trial, starting only with Si atoms, was close to the correct solution, except that one atom and its mirror had to be readjusted to a special position. A second trial with SiO_4 tetrahedra immediately found the correct T-site positions for 72 out of 76 T atoms in the unit cell.

A partial single crystal X-ray structure analysis was also carried out on the as-synthesized material. The single crystal model is very similar to the powder model except that there is a fifth T site within the $[6^45^34^33]$ cage (a cage containing 4 six-rings, 3 five-rings, 3 four-rings and 1 three-ring), corresponding to a density site identified earlier from the electron diffraction determination. Thus the three silanol positions within this cage are reduced to one on the symmetry axis. Refinement of only the framework atoms (59 parameters) resulted in a reasonable match, $R = 0.0680$, to all 2,451 measured reflections and $R = 0.0680$ to the 1,741 most intense reflections. Because of the usual symmetry disparity between framework architecture and the SDA, no attempt was made to refine the SDA geometry with this dataset.

The coordinates of the five T-site model were then geometrically refined using the prescribed distances estimated from the bulk composition of ITQ-40 (Si/Ge = 1.35, i.e., T-O = 1.67 Å, O-T-O = 109.524°, and T-O-T = 140° with relative weights of 1.0, 0.6, and 0.2, respectively). The final distance least squares (DLS) refined model had $R_{DLS} = 0.006$, indicating a suitable structure.

It was apparent that one of the T sites (T5 in the $[6^45^34^33]$ cage) was incompletely connected to other framework sites, requiring the presence of ≡Si-OH moieties (Q3 T atom). This has been detected by solid-state NMR measurements (Fig. 2). Regions representing silanols are preferentially enhanced in the CPMAS NMR spectrum (Fig. 2 *Inset*) and correspond to about 9.6% of the total MAS-NMR spectrum. Based on the chemical composition of Si/Ge = 1.35 (43.7 Si atoms/unit cell), this corresponds to 4.2 silanols/unit cell, very close to the expected 4 per unit cell anticipated from the model if this T site is occupied solely by silicon. The resultant framework also fits the electrostatic potential map found by direct phasing of the electron diffraction amplitudes (Fig. 4).

The solid-state ^{19}F NMR MAS spectrum was recorded on the as-synthesized sample of ITQ-40. As was stated before, the data indicate the presence of D4R and support higher framework Ge content, a ratio: Si/Ge ≈ 1 (Fig. 3). The ITQ-40 spectrum is at 6.55 ppm, to the left of the Si/Ge = 2 sample (at 8 ppm)—consistent with the Si/Ge ≈ 1 in ITQ-40.

It was found that ITQ-40 could be partially calcined in situ at 450 °C to remove 75% of the SDA without structural degradation. Therefore, the X-ray diffraction pattern of the partially calcined, dehydrated sample was measured from 3° to 40° 2-theta with CuKα radiation and 0.017 step size and subjected to Rietveld refinement starting with the coordinates from the geometrically optimized model. Soft restraints (74 total) were applied to the interatomic distances (T-O and O-O, but not T-T) and its relative weight factor could not be reduced below 50. If the soft restraints were removed, the overall goodness of fit, *Rwp*, only decreased from 0.0605 to 0.0570, and the interatomic bond angles and distances became unreasonable. The occupancy factors of tetrahedral atoms could not be refined to reasonable values, so they

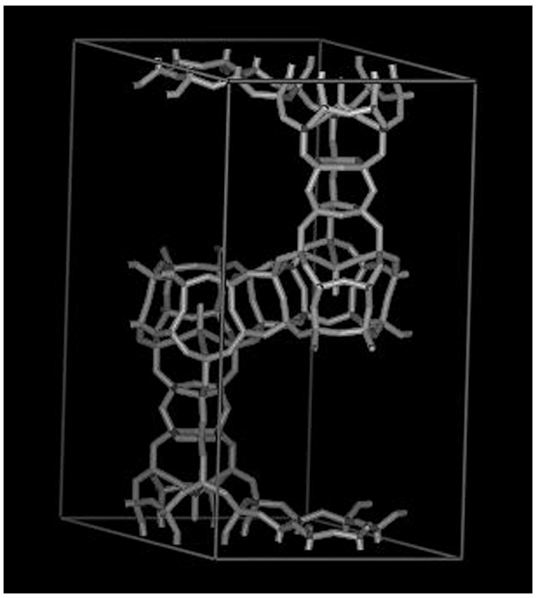

Fig. 5. Unit cell of calcined ITQ-40 from Rietveld refinement.

were fixed to the overall bulk chemical composition of Si/Ge≈ 1.35. With the final unit cell, $a = 16.469(2)$, $c = 32.192(5)$ Å, a final model (Fig. 5) was obtained corresponding to $Rwp = 0.0605$, $R(F^2) = 0.0638$ (Fig. 6). The crystallographic data from the refinement are given in Table 2 and final atomic coordinates are given in Table S1.

Because of the incomplete removal of the SDA from the pores, the inability of the soft restraints to be completely removed during refinement and the limitations of the X-ray powder data in being able to distinguish the distribution of the germanium sites within the structure, the final model is a good first approximation to the actual material. Nevertheless, the excellent fit of the experimental diffraction pattern to the calculated pattern after the Rietveld refinement along with the NMR analyses, as well as separate single crystal diffraction and electron diffraction determinations, as discussed above, all support the fact that the proposed framework model is correct.

Structural Description. The structure of ITQ-40 can be described as an interrupted, extra-large pore, three-dimensional zeolite framework with intersecting channels of 16 × 16 × 15-ring pores (Fig. 7). ITQ-40 is one of the very few zeolitic frameworks

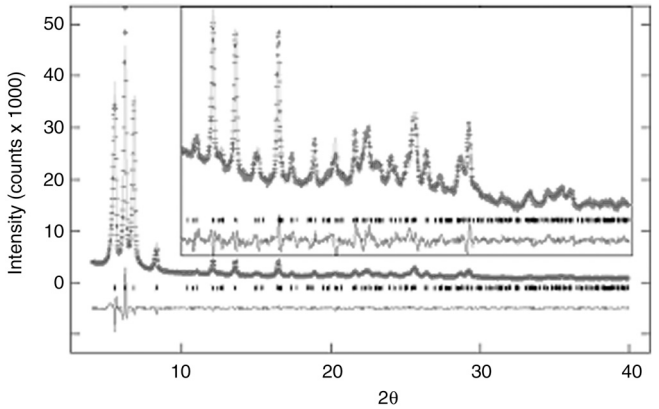

Fig. 6. Final plot from Rietveld refinement of calcined ITQ-40. The crosses are experimental data (Cu Kα radiation), the green line is the calculated pattern, the lower line is the difference curve, and markers indicate allowed reflections. (*Inset*) Intensity ×10.

Table 2. Crystallographic data for Rietveld refinement of calcined ITQ-40

Molecular formula	$[Ge_{32.4}Si_{43.6}O_{150}(OH)_4]$
Formula weight	6,044.3
a,b	16.469(2) Å
c	32.192(5) Å
α,β	90°
γ	120°
V	7562(2) Å^3
Z	1
Space group	$P6_3/mmc$ (no. 194)
T	303 K
λ	CuKα
Nobs	2,249
R_F2	0.0638
χ^2	9.544
Rwp	0.0605
Expected *Rwp*	0.0196

$Rwp = \{\Sigma w(Io\text{-}Ic)^2/\Sigma wIo^2\}^{1/2}$; $Rp = \Sigma|Io\text{-}Ic|/\Sigma Io$; $\chi 2 = \Sigma w(Io\text{-}Ic)^2/Nobs—Nvar$; expected $Rwp = Rwp/\{\chi 2\}^{1/2}$. Io = observed intensity of each point; Ic = calculated intensity of each point; *w* is the weight of each point.

containing extra-large (>12 T atoms) pores that run along more than one crystallographic direction. The gallium phosphate material cloverite (-CLO) (28) is the other one, but it contains three-dimensional 20-ring pores lined with dangling hydroxyl groups, and ITQ-37 (16) has a three-dimensional 30-ring pore system. Assuming an oxygen radius of 1.35 Å, the size of the near circular 15-ring pore that runs parallel along the *c* axis is 9.9 Å, and the size of the 16-ring pores that run parallel along the *a* and *b* axes is 9.4 Å × 10.4 Å, which is qualitatively in agreement with the information given by Ar adsorption.

The framework is built from three primary SBUs consisting of (*i*) $[6^45^34^33]$ cages connected along the *a* and *b* axes by (*ii*) D4Rs, $[4^6]$, and along the *c* axis by (*iii*) D3Rs, $[4^33^2]$. As suggested by electron diffraction, the arrangement of the SBUs and pores in ITQ-40 are similar to that present in the UCSB-8Co (**SBE**) and **EMT** frameworks, both having $P6_3/mmc$ symmetry and three-dimensional 12-ring pore systems. In **SBE**, the $[6^45^34^33]$

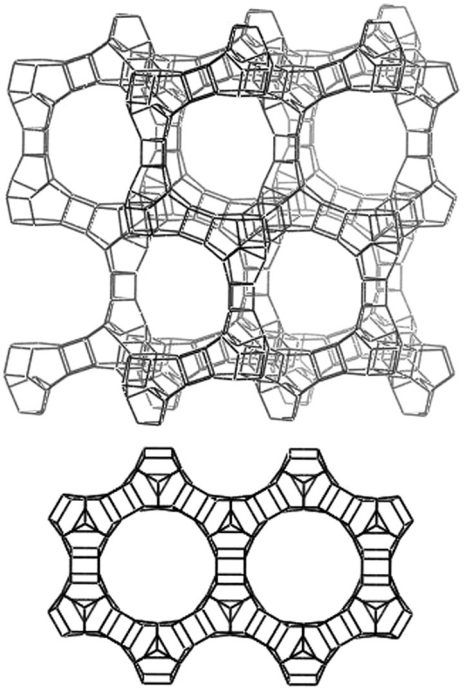

Fig. 7. Framework of ITQ-40. (*Upper*) View along the [100] direction showing the 16-ring pores. (*Lower*) View along the [001] direction showing the 15-ring pores. Oxygen atoms are not shown for clarity.

cages are replaced with cancrinite SBUs (*can*, $[6^5 4^6]$) that are connected by double six-rings (D6R, $[6^2 4^6]$) along the *c* axis and stilbite SBUs (*sti*, $[64^4]$) along the *a* and *b* axes, whereas in the **EMT** framework, sodalite cages (*sod*, $[6^8 4^6]$) are connected by D6Rs along all three axes.

As discussed above, although D3R SBUs have been observed in organic-containing silicate clathrates (17) and as molecular species in silicate mixtures [especially those with tetraethylammonium cations (18)], D3Rs have not previously been incorporated into a zeolite framework. As expected, the T-O-T angles associated with the D3R are smaller than those normally associated with D4Rs (130°–150°). In ITQ-40 the D3R T-O-T angles were all found to be smaller than 130°, i.e., T4-O20-T4 = 127.4°, T4-O19-T4 = 123.0°, and T4-O17-T3 = 128.7° (Table S2). In the clathrate, $(NEt_4)_6[Si_6O_{15}] \cdot 41H_2O$, the D3R T-O-T angles ranging from 129.6° to 132.5° were found from a single crystal structure determination (17). We propose that, similar to D4R geometry, the D3R T-O-T angles are relaxed by the presence of the germanium atoms, which have larger ionic radii than silicon, allowing for the more acute T-O-T angles. It must be mentioned, however, that the T-O-T angles determined from this refinement are to some extent correlated to the T-O and O-O distances by the soft restraints applied to them during the Rietveld refinement.

The resultant framework not only contains very large porous openings, i.e., 15-member rings parallel to the [001] hexagonal axis and 16-member ring channels perpendicular to this axis, it also has an extremely low framework density, 10.1 T/1,000 Å^3. This is lower than any other zeolitic framework except for a sulfide framework UCR-20 (**RWY**) (5.2 T/1,000 Å^3) (29), which is built entirely from three-member rings. Although the nonframework space of ITQ-40 is somewhat similar in **EMT** and **SBS**, their framework densities (respectively, 12.9 and 12.8 T/1,000 Å^3) are higher and neither contains three-member rings. The framework density of the -CLO framework (11.1 T/1.000 Å^3) containing three-dimensional 20-ring channels is also higher than ITQ-40, and only ITQ-37 (10.3 T/1,000 Å^3) containing tridimensional 30-ring channels approaches that of ITQ-40.

In recent years, several groups have generated a large number of theoretical zeolite structures, many containing extra-large pores (>12 T atoms). The existence of silicate structures containing 16-membered pore openings has been suggested by Curtis and Deem (30), who propose that these structures are thermodynamically accessible. While there are several known phosphate materials with 16-ring pore openings such as the gallium phosphates ULM-5 (31) and ULM-16 (32), as well as the iron phosphate ULM-15 (33), ITQ-40 represents a silicate material to have such pores.

Conclusions

An open zeolitic framework has been synthesized that contains both D4R and D3R as secondary building units. These generate the lowest framework density observed among the silicate zeolites, while leaving a tridimensional system of extra-large intersecting channels of $16 \times 15 \times 15$ ring pores. The synthesis of ITQ-40 shows that it is feasible to build zeolitic structures containing D3Rs, opening the possibility of synthesizing crystalline micro and even mesoporous materials with extra-large pores and very low framework densities.

Materials and Methods

Synthesis of ITQ-40 Zeolite. ITQ-40 zeolite has been synthesized either as a germanosilicate or as a germanoaluminosilicate using diphenyldiethylphosphonium hydroxide (Et_2Ph_2POH) as SDA. More specifically, a typical synthesis of ITQ-40 as germanosilicate is as follows: Germanium oxide was dissolved in a diphenyldiethylphosphonium hydroxide solution under stirring. Then, tetraethylorthosilicate was hydrolyzed in that solution and then stirred at room temperature to evaporate ethanol and water until the gel composition was reached. The gel composition was

$$0.5\,SiO_2 : 0.5\,GeO_2 : 0.4\,SDA(OH) : 0.4\,NH_4F : 1\,H_2O.$$

The gel was heated for one day at 175 °C in Teflon-lined stainless steel autoclaves under static conditions. The product was ITQ-40 with a Si/Ge ratio of 1.35.

The synthesis of the germanoaluminosilicate ITQ-40 was prepared by dissolving germanium oxide in a diphenyldiethylphosphonium hydroxide solution under stirring. Then, aluminum isopropoxide was hydrolyzed in that solution under stirring at room temperature. Finally, colloidal silica (40% SiO_2, duPont Ludox AS-40) and NH_4F were added and the gel stirred until evaporation of the excess water was completed. The final composition of the gel was

$$0.5\,SiO_2 : 0.5\,GeO_2 : 0.025\,Al_2O_3 : 0.4\,SDA(OH) : 0.4\,NH_4F : 1\,H_2O.$$

The gel was heated at 175 °C in Teflon-lined stainless steel autoclaves for 1 day under static conditions. The solid was filtered, washed, and dried at 100 °C, and the X-ray pattern showed that it corresponded to ITQ-40. The Si/Ge and T^{IV}/T^{III} ratio were 1.40 and 25, respectively.

Powder X-Ray Diffraction. Bragg–Brentano (reflection geometry) X-ray diffraction measurements of the as-synthesized ITQ-40 were made on a PANalytical X-Pert Pro laboratory instrument with Cu Kα radiation and X'Celerator solid-state detector with no monochromator. X-ray diffraction patterns were indexed with the Jade software package from MDI, Inc. Rietveld refinements of the structural models were made with General Structure Analysis System (34). Silicate models used for Rietveld refinement were first refined by DLS (35) to optimize bonding parameters.

Electron Diffraction. Transmission electron diffraction measurements on the as-synthesized material were carried out at 300 kV with a FEI/Philips CM-30 instrument. The zeolite sample was first crushed to a fine powder in a mortar and pestle and then suspended in acetone in an ultrasonic bath. Drops of the fine particle suspension were then dried on carbon-film-covered 300-mesh copper electron microscope grids. Later, microcrystalline preparations were also suspended in LR White resin and then sectioned with a Reichert–Jung Ultracut E-2 ultramicrotome. The sections were cut with a diamond knife and floated onto a water surface to be picked up with 200-mesh Cu grids covered with a holey carbon film.

Selected area electron diffraction patterns were recorded on Kodak Biomax MS X-ray film developed in Kodak GBX developer. Reciprocal spacings in diffraction patterns were calibrated against a gold powder standard.

Upon obtaining useful electron diffraction patterns (e.g., hk0 and 0kℓ), resultant films were digitized on a flatbed scanner, and these records were analyzed with the program ELD (36, 37) in the computer package CRISP (38) to extract intensities of the individual diffraction spots. No Lorentz correction was applied to these data. Attempts at direct structure analysis with these electron diffraction intensities were made using maximum entropy and likelihood via the computer program MICE (39).

Single Crystal Data Collection and Analysis. Colorless plate crystals of the as-synthesized ITQ-40 (minimum dimension 0.01 mm; maximum dimension 0.08 mm) were used for single crystal data collection on a Bruker diffractometer using MoKα X radiation via a graphite monochromator. The crystal structure was solved by direct methods using the SIR97 program package (40). The framework model was refined against measured data by full matrix least squares, using the SHELXTL (41) programs.

Solid-State Nuclear Magnetic Resonance. Multinuclear, ^{19}F, ^{31}P, ^{27}Al, and ^{29}Si, NMR spectra were recorded on the as-synthesized material at room temperature with an 11.7-T Varian *InfinityPlus* 500 (IP-500) spectrometer corresponding to Larmor frequencies of 470, 202, 130, and 99 MHz, respectively. The ^{19}F MAS-NMR spectrum was recorded on a sample loaded in a 3.2-mm (o.d.) ZrO_2 MAS rotor spinning at 20 kHz with a 60° pulse and a 30-s pulse delay. For ^{27}Al and ^{31}P NMR, the samples were loaded in 4-mm (o.d.) ZrO_2 MAS rotors and spun at the magic angle at rates of 10–16 kHz. The ^{27}Al MAS-NMR spectra were obtained with a $\pi/12$ rad pulse length and a recycle delay of 0.3 s. The ^{31}P MAS spectra were obtained with a $\pi/4$ rad pulse length and a recycle delay of 300 s. The ^{29}Si CPMAS and MAS-NMR spectra were recorded on samples loaded in 7.5-mm (o.d.) ZrO_2 MAS rotors spinning at 3.5 kHz and 4.5 kHz, with 3-s and 120-s pulse delays, respectively. The CP contact time in the CPMAS experiment was 3.5 ms. The ^{31}P, ^{27}Al, and ^{29}Si NMR spectra were recorded with ^1H

decoupling during data acquisition, and the chemical shifts are referenced with respect to external solutions of C_6F_6 ($\delta_F = -163$ ppm), $Al(H_2O)_6^{3+}$ ($\delta_{Al} = 0.0$ ppm), 85% H_3PO_4 ($\delta_P = 0.0$ ppm), and tetramethylsilane (TMS, $\delta_{Si} = 0.0$ ppm), respectively.

The ^{13}C MAS-NMR spectra were recorded using a 5-mm Chemagnetics probe on a Chemagnetics spectrometer operating at 4.7 T (^1H at 199.2 MHz) corresponding to a Larmor frequency of 50.2 MHz. ^{13}C CPMAS and MAS-NMR spectra were recorded at spinning speeds of 4.3 kHz and 8 kHz, respectively. A contact time of 1 ms and a pulse delay of 2 s were used in the CPMAS, and the pulse delay for the MAS experiment was 90 s. The ^{13}C NMR spectra are referenced against an external TMS ($\delta_C = 0.0$ ppm), using hexamethyl benzene as an external secondary standard and setting the aliphatic peak at 17.36 ppm.

SI Text. *SI Text* contains SDA synthesis details, table of atomic coordinates, interatomic distances and angles, pore distribution from Ar absorption, X-ray diffraction patterns of samples from ITQ-40 syntheses using Et_2Ph_2POH as SDA, ^{31}P, ^{27}Al, MAS-NMR and ^{13}C NMR of as-synthesized ITQ-40, and a cif file of atomic coordinates and unit cell parameters.

ACKNOWLEDGMENTS. The authors acknowledge the assistance of D. A. Sysyn and C. E. Chase in obtaining the NMR data.

1. Corma A (2003) State of the art and future challenges of zeolites as catalysts. *J Catal* 216:298–312.
2. Férey G (2001) Materials science: The simplicity of complexity—rational design of giant pores. *Science* 291:994–995.
3. Davis ME (2002) Ordered porous materials for emerging applications. *Nature* 417:813–821.
4. Corma A, Diaz U, Arrica M, Fernandez E, Ortega I (2009) Organic-inorganic nanospheres with responsive molecular gates for drug storage and release. *Angew Chem Int Edit* 48(34):6247–6250.
5. Brunner GO, Meier WM (1989) Framework density distribution of zeolite-type tetrahedral nets. *Nature* 337:146–147.
6. Cheetham T, et al. (2001) Very open microporous materials: From concept to reality. *Stud Surf Sci Catal* 135:788–795.
7. Annen MJ, Davis ME, Higgins JB, Schlenker JL (1991) VPI-7: The first zincosilicate molecular sieve containing three-membered T-atom rings. *J Chem Soc Chem Commun* 17:1175–1176.
8. McCusker LB, Grosse-Kunstleve RW, Baerlocher Ch, Yoshikawa M, Davis ME (1996) Synthesis optimization and structure analysis of the zincosilicate molecular sieve VPI 9. *Microporous Mater* 6:295–309.
9. Röhrig C, Gies H (1995) A new zincosilicate zeolite with nine-ring channels. *Angew Chem Int Edit* 34:63–65; *Angew Chem* 107:125–127.
10. Corma A, Navarro MT, Rey F, Rius J, Valencia S (2001) Pure polymorph C of zeolite beta synthesized by using framework isomorphous substitution as a structure-directing mechanism. *Angew Chem Int Edit* 40:2277–2280; *Angew Chem* 113:2337–2340.
11. Blasco T, et al. (2002) Preferential location of Ge in the double four-membered rings units of ITQ-7 zeolite. *J Phys Chem B* 106:2634–2642.
12. Dorset DL, et al. (2008) Crystal structure of ITQ-26, a 3D framework with extra-large pores. *Chem Mater* 20:5325–5331.
13. Dorset DL, et al. (2006) P-derived organic cations as structure-directing agents: Synthesis of a high-silica zeolite (ITQ-27) with a two-dimensional 12-ring channel system. *J Am Chem Soc* 128:8862–8867.
14. Corma A, et al. (2008) A zeolitic structure (ITQ-34) with connected 9- and 10-Ring channels obtained using phosphonium cations as structure directing agents. *J Am Chem Soc* 130:16482–16483.
15. Corma A, Díaz-Cabañas MJ, Jorda JL, Martínez C, Moliner M (2006) High-throughput synthesis and catalytic properties of a molecular sieve with 18- and 10-member rings. *Nature* 443:842–845.
16. Sun J, et al. (2009) *Nature* 458:1154–1157.
17. Wiebcke M, Felsche J (2001) The tetraethylammonium cation in a double three-ring silicate heteronetwork clathrate and a polyhedral clathrate hydrate: low-temperature single-crystal X-ray diffraction studies on $(NEt_4)_6[Si_6O_{15}] \cdot 40.8H_2O$ and $NEt_4OH \cdot 9H_2O$. *Microporous Mesoporous Mater* 43:289–297.
18. Pelster SA, Weimann B, Schaack BB, Schrader W, Schüth F (2007) Dynamics of silicate species in solution studied by mass spectrometry with isotopically labeled compounds. *Angew Chem Int Edit* 46:2299–2302.
19. Horvath G, Kawazoe K (1983) Method for the calculation of effective pore size distribution in molecular sieve carbon. *J Chem Eng Jpn* 16:470–475.
20. Caullet P, Guth JL, Hazm J, Lamblin JM, Gies H (1991) Synthesis, characterization and crystal structure of the new clathrasil phase octadecasil. *Eur J Sol State Inor* 28:359; Guth JP, et al. (1993) F-: A multifunctional tool for microporous solids—mineralizing, structure directing and templating effects in the synthesis. *Proceedings of the 9th International Zeolite Conference*, eds R Von Ballmoos, JB Higgins, and MMJ Treacy Vol I (Butterworth-Heinemann, London), pp 215–222.
21. Hahn Th, ed. (1995) International Tables for Crystallography. *Volume A Space Group Symmetry* (Kluwer, Dordrecht).
22. LeBail A, Duroy H, Fourquet JL (1988) The ab-initio structure determination of lithium antimony tungstate (LiSbWO6) by x-ray powder diffraction. *Mater Res Bull* 23:447–452.
23. Grosse-Kunstleve RW, McCusker LB, Baerlocher Ch (1999) Zeolite structure determination from power diffraction data: Applications of the FOCUS method. *J Appl Crystallogr* 32:536–542.
24. Bu X, Feng P, Stucky G (1997) Large-cage zeolite structures with multidimensional 12-ring channels. *Science* 278:2080–2085.
25. Baerlocher Ch, McCusker LB, Chiapetta R (1994) Location of the 18-crown-6 template in EMC-2 (EMT) Rietveld refinement of the calcined and as-synthesized form. *Microporous Mater* 2:269–280.
26. Engel GE, Wilke S, König O, Harris KDM, Leusen FJJ (1999) PowderSolve—a complete package for crystal structure solution from powder diffraction patterns. *J Appl Crystallogr* 32:1169–1179.
27. Deem MW, Newsam JM (1992) Framework crystal structure solution by simulated annealing: test application to known zeolite structures. *J Am Chem Soc* 144:7189–7198.
28. Estermann M, McCusker LB, Baerlocher Ch, Merouche A, Kessler H (1991) A synthetic gallophosphate molecular sieve with a 20-tetrahedral-atom pore opening. *Nature* 352:320–323.
29. Zheng N, Bu X, Wang B, Feng P (2002) Microporous and photoluminescent chalcogenide zeolite analog. *Science* 298:2366–2369.
30. Curtis RA, Deem MW (2003) A Statistical Mechanics Study of Ring Size, Ring Shape, and the Relation to Pores Found in Zeolites. *J Phys Chem B* 107:8612–8620.
31. Loiseau T, Férey G (1994) Oxyfluorinated microporous compounds VII. Synthesis and crystal structure of ULM-5, a new fluorinated gallophosphate $Ga_{16}(PO_4)_{14}(HPO_4)_2(OH)_2F_7$, $[H_3N(CH_2)_6NH_3]_4$, 6 H_2O with 16-membered rings and both bonding and encapsulated F. *J Solid State Chem* 111:403–415.
32. Loiseau T, Férey G (1996) Synthesis and crystal structure of ULM-16, a new open-framework fluorinated gallium phosphate with 16-ring channels: $Ga_4(PO_4)_4F_2 \cdot 1.5\,NC_6H_{14} \cdot 0.5\,H_2O \cdot 0.5\,H_3O$. *J Mater Chem* 6:1073–1074.
33. Cavellec M, Riou D, Grenèche JM, Férey G (1997) Oxyfluorinated compounds with an open structure: XVI synthesis, structure determination and magnetic properties of $Fe_4F_3(PO_4)(HPO_4)_4(H_2O)_4(N_2C_3H_{12})$ [ULM-15].. *Microporous Mater* 8:103–112.
34. Larsson AC, von Dreele RB (1994) *General Structure Analysis System, GSAS* (Los Alamos Laboratory, Los Alamos, NM).
35. Baerlocher Ch, Hepp A, Meier WM (1977) *Distance Least Squares Refinement Program, DLS-76* (ETH, Zürich).
36. Zou XD, Sukharev Y, Hovmöller S (1993) ELD—a computer program system for extracting intensities from electron diffraction patterns. *Ultramicroscopy* 49:147–158.
37. Zou XD, Sukharev Y, Hovmöller S (1993) Quantitative electron diffraction—new features in the program system ELD. *Ultramicroscopy* 52:436–444.
38. Hovmöller S (1992) CRISP: Crystallographic image processing on a personal computer. *Ultramicroscopy* 41:121–135.
39. Gilmore CJ, Bricogne G (1977) MICE computer program. *Method Enzymol* 277:65–78.
40. Altomare A, et al. (1999) SIR97: A new tool for crystal structure determination and refinement. *J Appl Crystallogr* 32:115–119.
41. Sheldrick G (2008) A short history of SHELX. *Acta Crystallogr* A64:112–122.